

1 **A database of radiogenic Sr-Nd isotopes at the “three poles”**

2 Zhiheng Du^a, Jiao Yang^a, Lei Wang^b, Ninglian Wang^c, Anders Svensson^d, Zhen
3 Zhang^e, Xiangyu Ma^f, Yaping Liu^a, Shimeng Wang^a, Jianzhong Xu^a, Cunde Xiao^{b*}

4 ^aState Key Laboratory of Cryospheric Science, Northwest Institute of
5 Eco-Environment and Resources, Chinese Academy of Sciences, Lanzhou 730000,
6 China

7 ^bState Key Laboratory of Earth Surface Processes and Resource Ecology, Beijing
8 Normal University, Beijing 100875, China

9 ^cCollege of Urban and Environmental Sciences, Northwest University, Xi’an 710127,
10 China

11 ^dCentre for Ice and Climate, Niels Bohr Institute, University of Copenhagen,
12 Copenhagen, Denmark

13 ^eSchool of Spatial Informatics and Geomatics Engineering, Anhui University of
14 Science and Technology, Huainan 232001, China

15 ^fQingdao Blue Thinking Information Technology Co.Ltd, Qingdao 266555, China

16 *Correspondence and requests for materials should be addressed to CD. X
17 (cdxiao@bnu.edu.cn).

18 **Abstract:** The radiogenic isotope compositions of strontium (Sr) and neodymium (Nd)
19 on the surface of the Earth are powerful tools for tracing dust sources and sinks on
20 Earth’s surface. To differentiate between the spatial variabilities of aeolian dust
21 sources in key cryospheric regions at the three poles (including the ‘Third Pole’
22 covering the high mountainous area in Asia, the Arctic and Antarctica), a dataset of
23 the Sr-Nd isotopic compositions from the terrestrial extremely cold or arid
24 environments in this study was compiled, similar to the method of Blanchet (2019).
25 The database identified snow, ice, sand, soil (loess), sediment, and rock from the

26 modern and Quaternary periods of the three poles based on 90 different references and
27 our own measurement data, with a total of 1989 data points, 206 data points with
28 different grain sizes and 209 data points with fraction measurements. There are 485
29 data points from the Third Pole, 727 data points from the Arctic, and 777 data points
30 from Antarctica. The sampling and measurement methods of these data are introduced.
31 For each pole, geographical coordinates and other information are provided. The main
32 scientific purpose of this dataset is to provide collective documentation and our own
33 measurements for the Sr-Nd dataset, which will be useful for determining the sources
34 and transport pathways of dust in snow and ice, river, and oceans at the three poles,
35 and to investigate whether multiple dust sources are present at each of the poles. This
36 dataset provides exhaustive detailed documentation of the isotopic signatures at the
37 three poles during specific time intervals of the Quaternary period, which are useful
38 for understanding the sources or sinks of aeolian dust or sediments at the three poles.
39 The datasets are available from the National Tibetan Plateau Data Center
40 (<https://doi.org/10.11888/Cryos.tpd.272100>, Du et al., 2022).

41 **Keywords:** Radiogenic isotopic dataset, Third Pole, Arctic Ocean, Greenland and
42 Antarctic ice sheets, Dust provenances.

43 **1. Introduction**

44 The role of mineral dust in the Earth system extends well beyond its impact on
45 the energy balance and involves interactions with the carbon cycle and glacier melting
46 on global scales (Skiles et al., 2018; Shao et al., 2011). The transport of dust from the
47 low mid-latitudes, which contain major deserts that are dust sources, to the Arctic
48 region or AIS is sensitive to amplified high-latitude climatic variability (Bory et al.,
49 2003a; Bory et al., 2003b; Lupker et al., 2010; Lambert et al., 2013; Struve et al.,
50 2020). The isotopic compositions of the radiogenic isotopes strontium (Sr) and

51 neodymium (Nd) are powerful tools for tracing dust sources and sinks because their
52 characteristics are significantly different on the surface of the Earth (including snow,
53 sand, sediment, loess and aeolian deposits) (Grousset et al., 2005; Chen et al., 2007;
54 Xu et al., 2012; **Robinson et al., 2021**). Therefore, the combination of different
55 isotopic signatures, specifically $^{87}\text{Sr}/^{86}\text{Sr}$ and $^{143}\text{Nd}/^{144}\text{Nd}$ (expressed as $\epsilon_{\text{Nd}}(0)$), has
56 proven to be useful in discriminating different dust source areas in Earth science.

57 The transport of aeolian dust from natural desert regions has also been identified
58 in modern snow and ice records at the third pole based on Sr-Nd data (Wu et al., 2010;
59 Xu et al., 2012; Du et al., 2015; Dong et al., 2018). Many studies have focused on
60 dust transport from the western Chinese deserts to the Chinese loess plateau (CLP),
61 Pacific Ocean and even the Greenland ice sheet (GrIS) (Biscaye et al., 1997; Chen et
62 al., 2007; Wei et al., 2021). However, it is still a controversial issue; for example,
63 recent results have emphasized that aeolian dust from local sources contributes
64 significantly to high mountain glaciers (Du et al., 2019a; Wei et al., 2021). And
65 aeolian dust from various source regions, including the Saharan Desert in North
66 Africa and the Gobi and Taklimakan Deserts in Asia, is transported to the Greenland
67 snow and ice, and there are still great uncertainties (Han et al., 2018).

68 The Sr-Nd data in snow layers at the Berkner Island ice sheet in western
69 Antarctica, for most of the year, are data support scenarios that involve contributions
70 from proximal sources (Bory et al., 2010). The Sr-Nd data from insoluble dust in
71 snow samples from East Antarctica indicate that long-distance natural dust primarily
72 originates from Australia and that local dust originates from ice-free areas (Du et al.,
73 2018). The Sr-Nd data in the Taylor Glacier zero-age ice samples and snow samples
74 from Roosevelt Island could be a mixture of at least two local sources (Winton et al.,
75 2016; Aarons et al., 2017). The Sr-Nd data from East Antarctica ice cores during the

76 Holocene indicate a well-mixed atmospheric background involving a mixture of two
77 or more sources in the Southern Hemisphere (SH) (Aarons et al., 2016, 2017;
78 Delmonte et al., 2019). The amount of isotopic information is currently adequate for
79 Patagonian and non-Patagonian mineral dust exported from southern South America
80 and the East Antarctic ice sheet (EAIS) (Grousset et al., 1992; Gaiero et al., 2007;
81 Delmonte et al., 2010a, b, 2019; Delmonte et al., 2013; Blakowski et al., 2016; Aarons
82 et al., 2017). Major efforts have attempted to solve the ‘puzzle’ of the origin of the
83 potential source areas that contribute dust to the Southern Ocean (SO) and the whole
84 Antarctic Ice Sheet (AIS) (Gili et al., 2021). However, Sr-Nd data in the entire AIS
85 have an uneven distribution. Measuring Sr-Nd stable isotopic compositions in ice
86 cores from Antarctica is a major challenge.

87 As much Sr-Nd data were measured, these data characteristics and measurement
88 methods, which is necessary to reassess these data on the dust sources in these remote
89 regions. Therefore, the amounts of Sr-Nd data measured in snow, soil, sediment, sand
90 and other samples should be integrated into a dataset to better serve the environmental
91 and climatic sciences studying the third regions in the future. The answers to these
92 questions have been hindered by a paucity of Sr-Nd data, which provide information
93 on the local and potential dust sources. For these reasons, we measured Sr-Nd data in
94 some samples and collected Sr-Nd data in the literature at the three poles (Fig. 1,
95 Table 1). Therefore, the objective of this work was to produce a compilation of
96 published and unpublished data from the three poles, and the specific time intervals of
97 Sr-Nd data were limited to the Quaternary period. As an example, the modern dust
98 (Holocene) in snow or ice and sediment sample contributions from the three poles
99 were further discussed, and the potential dust transport paths in Greenland and
100 Antarctic ice sheets were traced. Similar to the method of Blanchet (2019), here, we

101 compile published and unpublished Sr-Nd data with an integrated filtering system
102 from three remote poles, in which these data were collected in extremely cold or arid
103 environments, and most of the data were not included in the previous dataset. The
104 dataset will help trace modern natural dust, reconstruct past environments, and extend
105 the database of terrestrial and marine radiogenic Sr and Nd isotope data in the Earth
106 and environmental sciences.

107 **2. Sample measurement and data processing**

108 **2.1 Sample collection and measurement**

109 Sr-Nd data in snow, sand, soil, cryoconite, loess and sediment samples were
110 collected from our own research and literature from three poles (the ‘Third Pole’
111 covering the high mountainous area in Asia, the Arctic and Antarctica) (Fig. 1). Sr-Nd
112 data in the Third Pole cover the area of 40° to 23°N and 106° to 61°E and included
113 data from arid deserts and mountains in northern China (Fig. 2). Sr-Nd data in the
114 Arctic from the high Arctic to the sub-Arctic areas, and Sr-Nd data in Antarctica refer
115 to the area including the entire Antarctic continent, the AIS, and the Antarctic
116 Peninsula (>60°S). Sr-Nd data were collected from Australia, southern South America
117 (SSA), southern Africa (SA) and New Zealand (Fig. 1). The cryoconite samples
118 indicate that the mixtures and/or aggregates of these biotic and abiotic impurities on
119 glacial ice, were collected at different elevations in glaciers (Table 2). Note that the
120 Sr-Nd data from the snow, ice core, surface aeolian dust, deposit samples, and the
121 ages of these samples are almost all less than one million. Therefore, the ages of
122 Sr-Nd data are limited to the Quaternary period in this dataset.

123 Two sand samples from Kangerlussuaq, West Greenland were collected. Four
124 sand samples collected on King George Island and eleven sand samples collected on
125 Inexpressible Island in the Ross Sea, West Antarctica, were measured in this study. In

126 general, the upper 2 or 5 cm of surface topsoil (sand) was collected with a trowel and
127 stored in precleaned plastic bags or bottles. The sediment samples from shelves and
128 ridges in the Arctic Ocean (AO), which were mostly retrieved from core archives,
129 were subsampled in the upper surface of the core tops (with rare exceptions) (Maccali
130 et al., 2018). Different grain sizes ($<5\ \mu\text{m}$, $<10\ \mu\text{m}$, $30\ \mu\text{m}$, $<63\ \mu\text{m}$, $<75\ \mu\text{m}$ and <100
131 μm fractions and bulk) of surface soil or sand were extracted by the sieving method
132 (Chen et al., 2007; Maccali et al., 2018; Du et al., 2018, 2019a, b; Wei et al., 2021).

133 Snow samples were collected from the snowpit at a vertical resolution of 5–20
134 cm, following the clean-hands protocol with sampling personnel wearing integral
135 Tyvek[®] bodysuits, nonpowdered gloves and masks to avoid possible contamination
136 (Xu et al., 2012). In this study, one 1.0 m snowpit with a resolution of 10 cm was dug
137 in the East Greenland ice sheet (GrIS), and four fresh snow samples (M1, M2, M3 and
138 M4) were sampled on sea ice in the Arctic Ocean (AO) during fulfil mission of the
139 Multidisciplinary drifting Observatory for the Study of Arctic Climate (MOSAIC) in
140 October 2020. Surface fresh snow (2-10 cm) samples at different resolutions (with
141 different thicknesses, widths and lengths) in Greenland and Antarctica ice sheets were
142 excavated and placed in 5 L Whirl-Pak bags (Du et al., 2018; Du et al., 2019a, b).
143 Three horizontal snow layers were collected for Greenland and Antarctica snowpits
144 (Bory et al., 2003b; Bory et al., 2010). The dust in the ice core was extracted using the
145 same method as that for the snow samples. Snow or ice core samples are nearly bulk
146 samples or have different grain sizes ($>0.2\ \mu\text{m}$, $> 0.45\ \mu\text{m}$, $> 0.45\ \mu\text{m}$ and $<30\ \mu\text{m}$)
147 (Du et al., 2015, 2019b; Bory et al., 2003 a, b; Bory et al., 2010; Lupker et al., 2010;
148 Wu et al., 2010).

149 **2.2 Data processing**

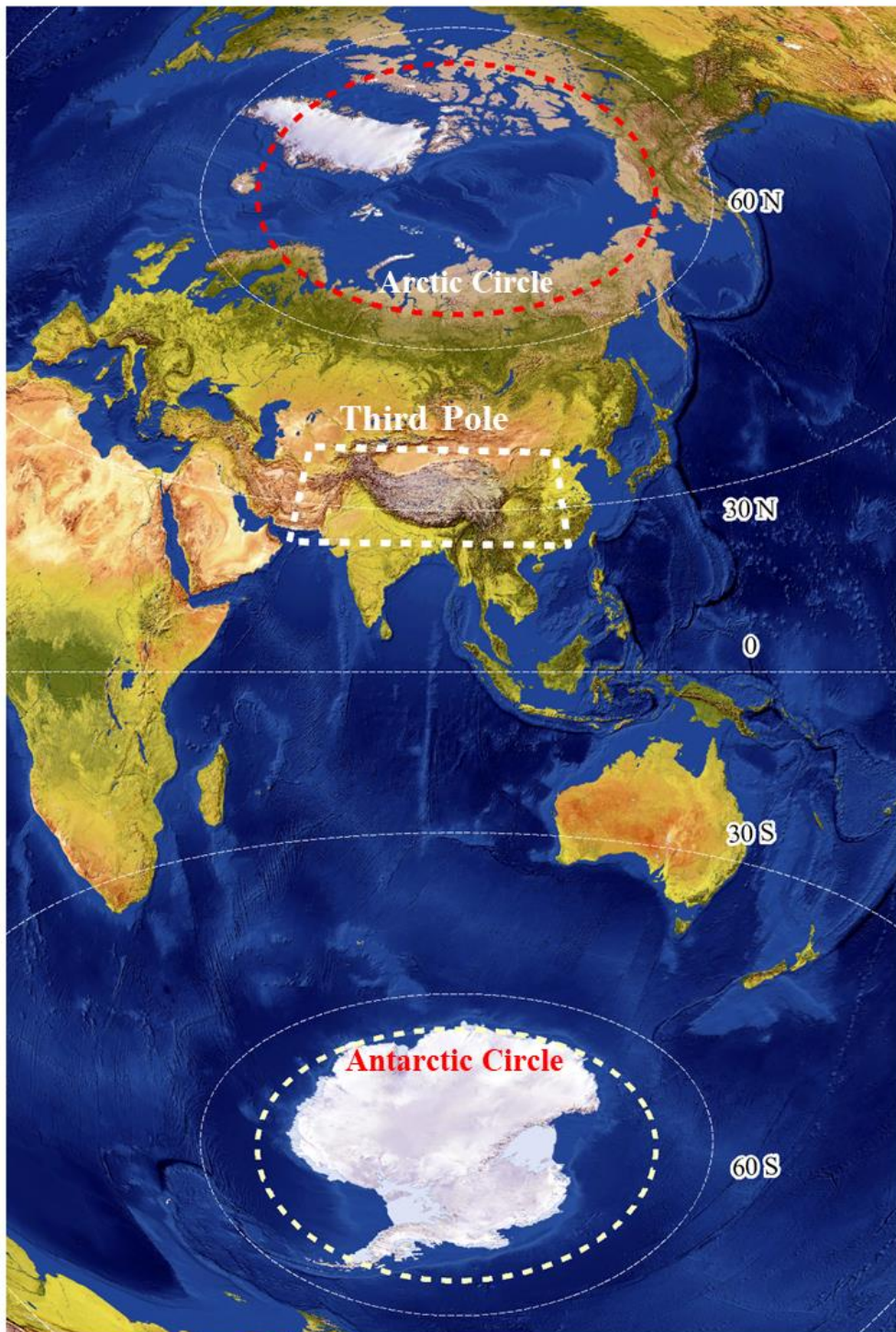
150 **Sr-Nd isotope datasets from snow, ice cores, sand, sediment, soil and loess**

151 samples from the Third Pole, Arctic and Antarctica were compiled. Data were
152 collected from 90 different references with 2844 data points. In total, 485 data points
153 were collected from the Third Pole, 727 data points were collected from the Arctic,
154 and 777 data points were collected from the Antarctica. In addition, 259 data points
155 were collected from the Pan-third pole, and 181 data points were included from the
156 potential source areas (PSAs) of SH. Details of geographical coordinates and original
157 information can be found in this dataset, and the locations of these samples are shown
158 on maps. To keep the naming scheme uniform, the dataset assembled the names of
159 each sample based on the work by Blanchet (2019). This dataset was built by
160 incorporating data from the literature and our own database; in particular, units,
161 source or sink and geographical coordinates are marked in the dataset. Note that the
162 Sr-Nd data whether represent source or sink information, which need determine based
163 on the detail depositional environment or distribution. For examples, the loess
164 samples from the CLP represent the sink, which it also represent the dust source for
165 the Pacific Ocean. Therefore, these samples were marked with mixture. And the
166 sediment samples from the coast of SO or AO (Rivers or Dune sand) were also
167 marked with mixture. An overview of the input data is shown in Table 1. The study
168 focuses on the large amounts of different data, including data on snow, ice, sand, soil,
169 loess, sediment, etc. The data are based on our own measurements, author
170 contributions (data published) and literature searches.

171 All subsequent procedures were performed in clean lab facilities. The sand, loess,
172 sediment, cryoconite and dust extracted from snow or ice cores were generally
173 digested with ultrapure acid (HNO_3 , HF and HClO_4 or HNO_3 , HF and HCl), and
174 $^{87}\text{Sr}/^{86}\text{Sr}$ and $^{143}\text{Nd}/^{144}\text{Nd}$ ratios were determined by the different types of
175 thermoionization mass spectrometry or multiple collector inductively coupled

176 plasma-mass spectrometry. Sr-Nd values, with uncertainties expressed as $\pm 2\sigma \times 10^{-6}$ (2
177 standard errors of the mean), can also be found in the original references. The
178 $^{143}\text{Nd}/^{144}\text{Nd}$ isotopic composition is expressed as:

179 $\epsilon_{\text{Nd}}(0) = ((^{143}\text{Nd}/^{144}\text{Nd})_{\text{Sample}} / (^{143}\text{Nd}/^{144}\text{Nd})_{\text{CHUR}} - 1) \times 10^4$, where $(^{143}\text{Nd}/^{144}\text{Nd})_{\text{CHUR}}$
180 = 0.512638, where CHUR stands for chondritic uniform reservoir and represents a
181 present-day average Earth value $(^{143}\text{Nd}/^{144}\text{Nd})_{\text{CHUR}} = 0.512638$ (Jacobsen &
182 Wasserburg 1980).



183

184 Fig. 1. Map of the sampling regions in the three poles (Third Pole: data were collected
 185 in the area of 40° to 23°N and 106° to 61°E, Li et al., 2020; Arctic: from the high
 186 Arctic to the sub-Arctic areas, data were collected >60°N in this region); and
 187 Antarctica: data were collected >60°S in this region, which are indicated with

188 different coloured circles) in this study (The background of this figure is from
189 ArcGIS).

190 3. Data descriptions

191 3.1. Reliability assessment for the differences in Sr-Nd based on grain sizes, 192 lithogenic and measuring methods

193 The grain size effect in different samples resulted in $^{87}\text{Sr}/^{86}\text{Sr}$ ratio and $\epsilon_{\text{Nd}}(0)$
194 variations. For surface aeolian sand and marine sediment samples, the variations in
195 size-separated $^{87}\text{Sr}/^{86}\text{Sr}$ values are slightly affected by grain size (Chen et al., 2007;
196 Tütken et al., 2002). The Sr isotope ratios in loess from the CLP tended to be higher in
197 the fine fraction and were much higher in the $<2 \mu\text{m}$ fraction than in other coarser
198 fractions (Rao et al., 2006). However, the variations in the $^{87}\text{Sr}/^{86}\text{Sr}$ isotopic ratios in
199 alpine soils of the Tibetan Plateau are not clearly related to the carbonate effect and
200 grain size effect (Lin and Feng, 2015). $\epsilon_{\text{Nd}}(0)$ values clearly exhibits the grain
201 size-dependent variability, because $\epsilon_{\text{Nd}}(0)$ values seem not to be fractionated between
202 mineralogically different grain-size fractions during the sedimentary cycle (Tütken et
203 al., 2002; Xie et al., 2020). While a substantial proportion of Sr-Nd isotope values
204 showed enrichment in the coarse-grained fraction ($< 63 \mu\text{m}$, $30\text{--}63 \mu\text{m}$, $10\text{--}30 \mu\text{m}$ and
205 $< 10 \mu\text{m}$) (Xie et al., 2020). Within the isotopically diverse Indus delta sediment, bulk
206 isotopic compositions are estimated to deviate on average no than $\pm 1.04 \epsilon_{\text{Nd}}$ units and
207 ± 0.0099 for $^{87}\text{Sr}/^{86}\text{Sr}$ values for any sediment as a result of mineralogy, grain size
208 distribution, and analytical error (Jonell et al., 2018)..

209 The $\epsilon_{\text{Nd}}(0)$ signatures of the lithic fraction of the sediments are taken as a robust
210 circulation and hydrologic proxies applicable because of its different origins across
211 timescales (Revel et al., 1996; Abbott et al., 2022). However, Sr-Nd isotope ratios in
212 the lithogenic sediment fraction represent a complex mixture (Meinhardt et al., 2016;

213 Bayon et al., 2021). The widespread influence of lithogenically sourced neodymium
214 on authigenic $\epsilon_{Nd}(0)$ had been demonstrated. Such as, there is a strong linear
215 relationship between detrital $\epsilon_{Nd}(0)$ and authigenic $\epsilon_{Nd}(0)$ ($r=0.86$, $n=871$). Therefore,
216 the sediment characteristics and detrital isotope records should be considered when
217 used $\epsilon_{Nd}(0)$ data (Abbott et al., 2022). The different acid leaching methods also have
218 an effect on the Sr-Nd isotopic composition in the silt and clay fractions in marine
219 sediments (Walter et al., 2000). Loess samples from the CLP and cryoconites
220 (including surface dust) from high mountain glaciers had obviously higher $^{87}Sr/^{86}Sr$
221 ratios after acid treatment than before (Rao et al., 2016; Nagatsuka et al., 2010,
222 Nagatsuka et al., 2019). In addition, $\epsilon_{Nd}(0)$ of the leachable in the surface sediment
223 samples implied the North Atlantic deep water circulation pattern. Sr-Nd data in
224 Fe-Mn fractions of marine sediments can be used in paleoceanography to infer
225 transportation of terrigenous material and changes in bottom-water circulation (Bayon
226 et al., 2002; Asahara et al., 2012).

227 Therefore, assuming that Sr-Nd data in different media in this dataset were used
228 for interpreting Sr-Nd isotope compositions in terms of provenance and
229 paleoceanography, the grain sizes, lithogenic and measurement methods on these
230 isotopic data must be considered for better illustration using these data.

231 3.2 The Sr-Nd data characteristics of glaciers at the Third Pole

232 Table 2 and Fig. 2 provide an overview of the information (the serial number of
233 glaciers; sub-regions; glacier name; name of the sampling site where the samples were
234 taken; sample type, age, elevation; longitude and latitude and elevation) from the
235 Third Pole. The dust in snow or ice in the Third Pole absolutely originates from PSAs,
236 therefore, Sr-Nd data in these samples represents the characteristics of sinks. And
237 Sr-Nd data from the local or arid deserts sand or soil represents the characteristics of

238 PSAs. As an example, the isotopic signatures in insoluble dust of these snow/ice
239 (sinks) from the Third Pole can be traced that which originate from the possible PSAs
240 based on those Sr-Nd data and geographic characteristics in sand (soil) samples from
241 the local exposed bedrock and long-distance dust transport of arid deserts. The same
242 Sr-Nd measurement methods were used in these snow samples (Xu et al., 2012; Du et
243 al., 2015, 2019a; Dong et al., 2018, Wei et al., 2019, 2021), and a similar
244 measurement method was used in those sand or surface dust samples (Chen et al.,
245 2007; Nagatsuka et al., 2010). The data results seem to remain fully consistent with
246 these references.

247 The sorting criteria for determining PSAs based on mountains and glaciers
248 distribution, geographic features and isotopic values (snow or ice from the Third Pole
249 glaciers, sand (soil) from local and arid deserts), six isotopic sub-regions across the
250 entire Third Pole were divided as follows (Fig. 2):

251 Region I: Samples from glaciers located in the Altai Mountains include snow
252 samples from Musidao glacier and Altay, and sand samples from the Gurbantunggut
253 Desert, with $\epsilon_{Nd}(0)$ values from -6.6 to -1.2 and $^{87}Sr/^{86}Sr$ values ranging from
254 0.705483 to 0.71480. The highest $\epsilon_{Nd}(0)$ values were observed in this region (Chen et
255 al., 2007; Xu et al., 2012; Du et al., 2019a).

256 Region II: Samples from the glaciers on the northern margin of the TP include
257 snow samples from the Tianshan Mountains (Tianshan No. 1 glacier and Miaoergou
258 ice cap) and Kunlun Mountains (Muztagata), as well as sand samples from the
259 Taklimakan Desert, with $\epsilon_{Nd}(0)$ values from -11.8 to -6.9 and $^{87}Sr/^{86}Sr$ values from
260 0.70842 to 0.728641 (Chen et al., 2007; Nagatsuka et al., 2010; Du et al., 2015; Xu et
261 al., 2012; Wei et al., 2019).

262 Region III: The Sr-Nd isotopic characteristics of the glaciers and sand/soil in the

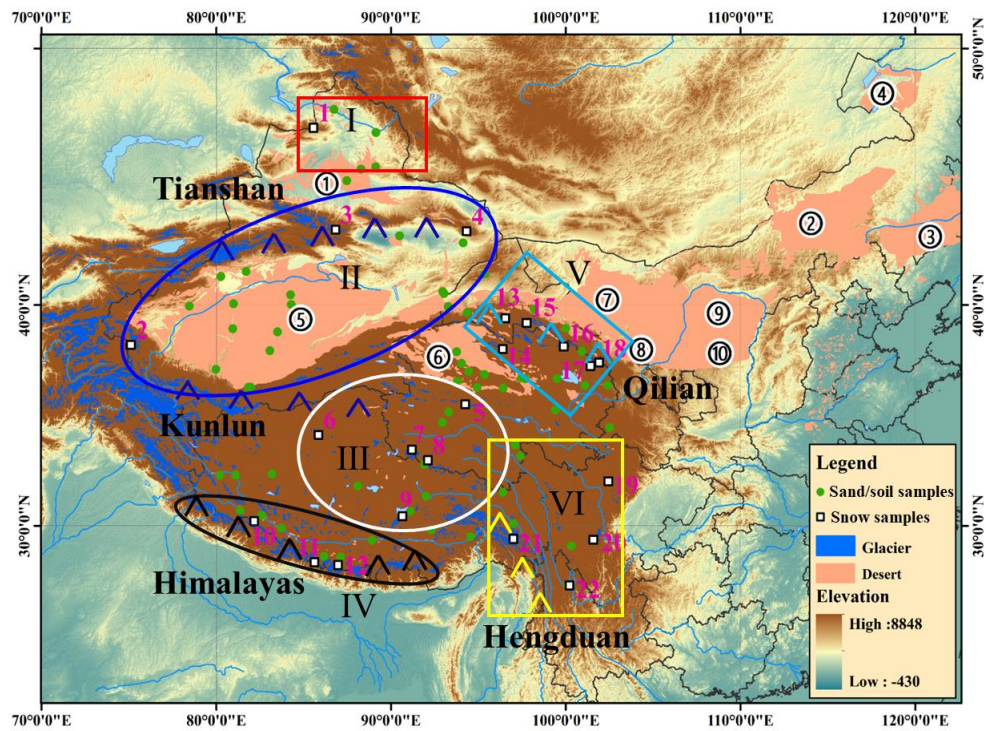
263 interior of the TP include $\epsilon_{\text{Nd}}(0)$ values ranging from -10.5 to -8.6 and $^{87}\text{Sr}/^{86}\text{Sr}$ values
264 from 0.713192 to 0.721786 (Xu et al., 2012; Du et al., 2019a; Wei et al., 2021).

265 Region IV: The Sr-Nd isotope data from snow and sand (soil) samples from
266 glaciers in the Himalayan Mountains (East Rongbuk, Jiemayangzong and Yala)
267 include $\epsilon_{\text{Nd}}(0)$ values ranging from -28.1 to -10.5 and $^{87}\text{Sr}/^{86}\text{Sr}$ values ranging from
268 0.724542 to 0.757407 (Xu et al., 2012; Wei et al., 2021).

269 Region V: Samples from the glaciers in the Qilian Mountains include snow
270 samples from the Qilian Mountains and sand (soil and loess) samples from the Hexi
271 Corridor, with $\epsilon_{\text{Nd}}(0)$ values from -15.7 to -7.0 and $^{87}\text{Sr}/^{86}\text{Sr}$ values from 0.712349 to
272 0.73211 (Wei et al., 2017; Dong et al., 2018). The $\epsilon_{\text{Nd}}(0)$ values have an increasing
273 trend along the Hexi Corridor from west to east: -15.7--12.9 for Laohugou No. 12
274 glacier (local soil: -13.6), -13.7--8.58 for Qiyi, -13.8--13.6 for Shiyi glacier (local
275 soil: -13.8--13.6), -12.1--12.0 for Dabanshan snowpack, and -10.9--7.0 for
276 Lenglongling glacier (Fig. 2, Dong et al., 2018). It is very clear that, based on local
277 soil data, regional dust makes a significant contribution to these glaciers.

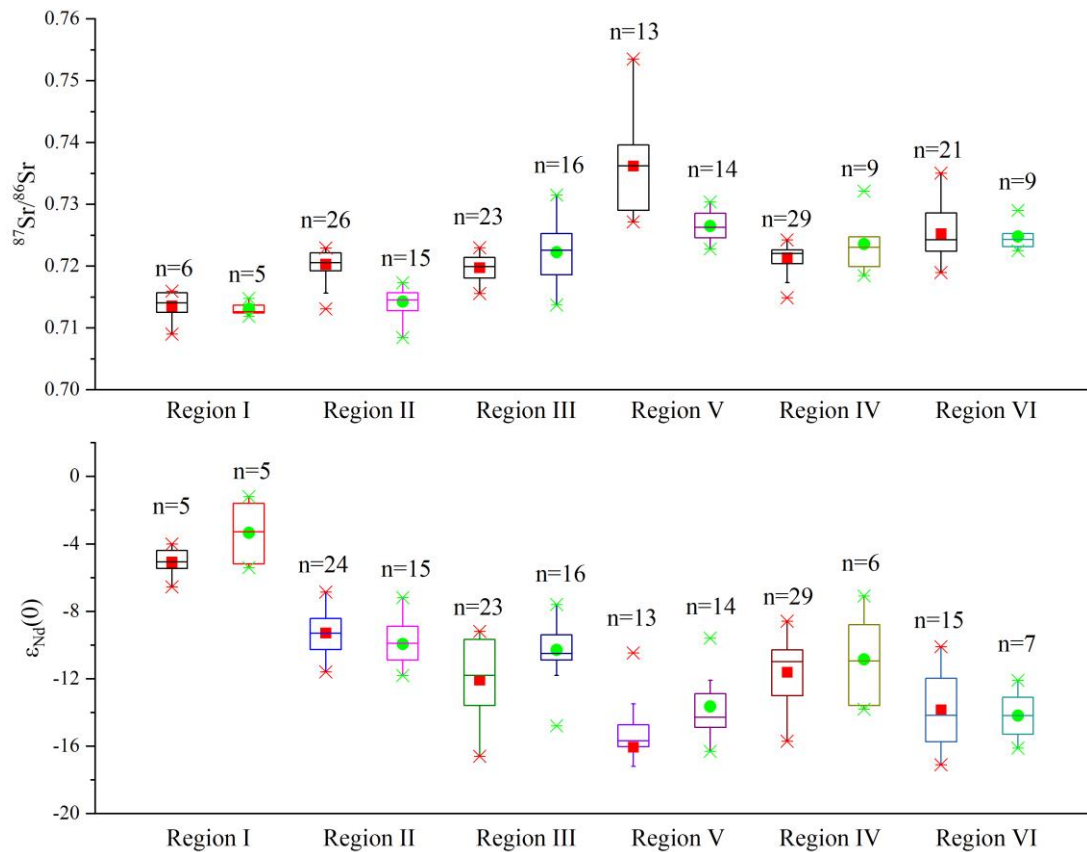
278 Region VI: Samples from the glaciers in the eastern TP include snow and soil
279 samples from the Hengduan Mountains, with $\epsilon_{\text{Nd}}(0)$ values from -17.1 to -10.1 and
280 $^{87}\text{Sr}/^{86}\text{Sr}$ values from 0.717145 to 0.735863 (Xu et al., 2012; Dong et al., 2018).

281 There is an increasing $^{87}\text{Sr}/^{86}\text{Sr}$ trend from north (region I) to south (region V),
282 and there is a decreasing $\epsilon_{\text{Nd}}(0)$ trend from north (region I) to south (region V). The
283 maximum $^{87}\text{Sr}/^{86}\text{Sr}$ ratios and minimum $\epsilon_{\text{Nd}}(0)$ values were observed in region V (Fig.
284 3). The Sr-Nd data in the Third Pole have relatively narrow ranges with distinct
285 features, while the largest uncertainty was observed from Region IV (Fig. 3).



286

287 Fig. 2. The glacier and desert distributions in western China (the different coloured
 288 oval and rectangular shapes represent six sub-regions (PSAs and glaciers) (Tianshan,
 289 Kunlun, Qilian, Himalayas and Hengduan Mountains) in the Third Pole; pink
 290 numbers and white rectangles represent 22 glaciers (snow samples were collected
 291 from these glaciers) for which the names of glaciers are shown in Table 2, and the
 292 numbered circles represent the ten deserts or sandy areas of China (1. Gurbantungut
 293 Desert, 2. Onqin Daga sandy land, 3. Horqin sandy land, 4. Hunlun Buir sandy land, 5.
 294 Taklimakan Desert, 6. Qaidam Desert, 7. Badain Jaran Desert, 8. Tengger Desert, 9.
 295 Hobq Desert, 10. Mu Us Desert), and green solid circles represent sand/soil samples
 296 (this figure was created with ArcGIS).



297

298 **Fig. 3.** Box plot for the Sr-Nd isotope signatures of third pole PSAs and snow samples.

299 Samples are located in each PSA region based on the data from Table 2 (the number

300 of samples for each sub-region are presented ($n > 5$)). The horizontal line within the

301 box is the median, and the squares are the mean Sr-Nd values (red rectangles for sand

302 or soil samples and green solid cycles for snow samples). The interquartile range is

303 represented by the lower and upper boundaries of the boxes, and whiskers indicate

304 confidence intervals of 1.5 times the interquartile range.

305 3.2. Sr-Nd data from the Arctic

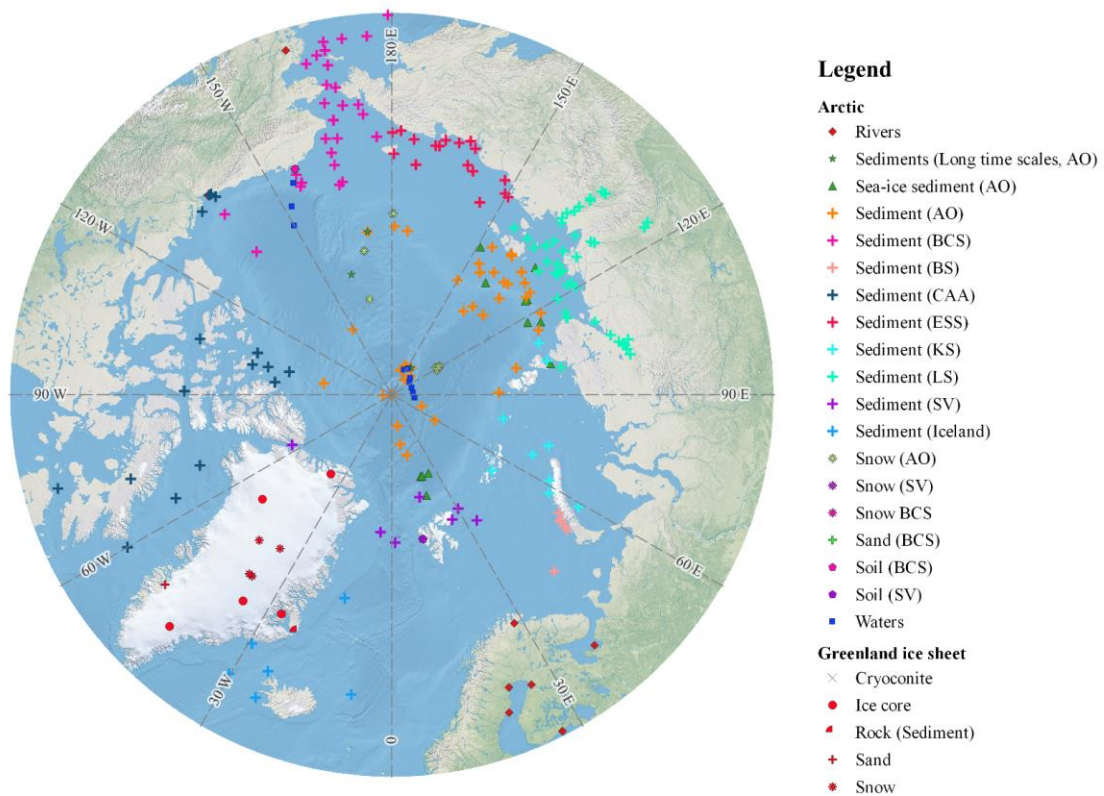
306 Considerable Sr-Nd data have been obtained from modern snow/ice samples from the

307 Arctic and surface (including sea ice-transported sediments) sediment from the AO,

308 which covers the entire Arctic and represents the characteristics of sinks (Fig. 4). The

309 data points are presented in Table 3. Sr-Nd data from arid deserts (East Asian and

310 Saharan deserts) have been compiled in previous datasets (Blanchet et al., 2019;
 311 Robinson et al., 2021), and these data are useful for tracing terrigenous material
 312 transport in the Arctic. For user-friendly selection of the Sr-Nd data according to the
 313 modern environment characteristics and the geographical location, Sr-Nd data from
 314 the deep ice core are not included in Fig. 5. We compared the Sr-Nd data from the
 315 surface snow (sink) and marine sediment (sink or source) samples in the Arctic (Figs.
 316 5 and 6). Based on the isotopic signals of these samples, geologic units, adjacent seas
 317 and drainage basins of the main river systems in the Arctic, the Sr-Nd patterns can be
 318 divided into 12 sub-regions according to Maccali et al. (2018).



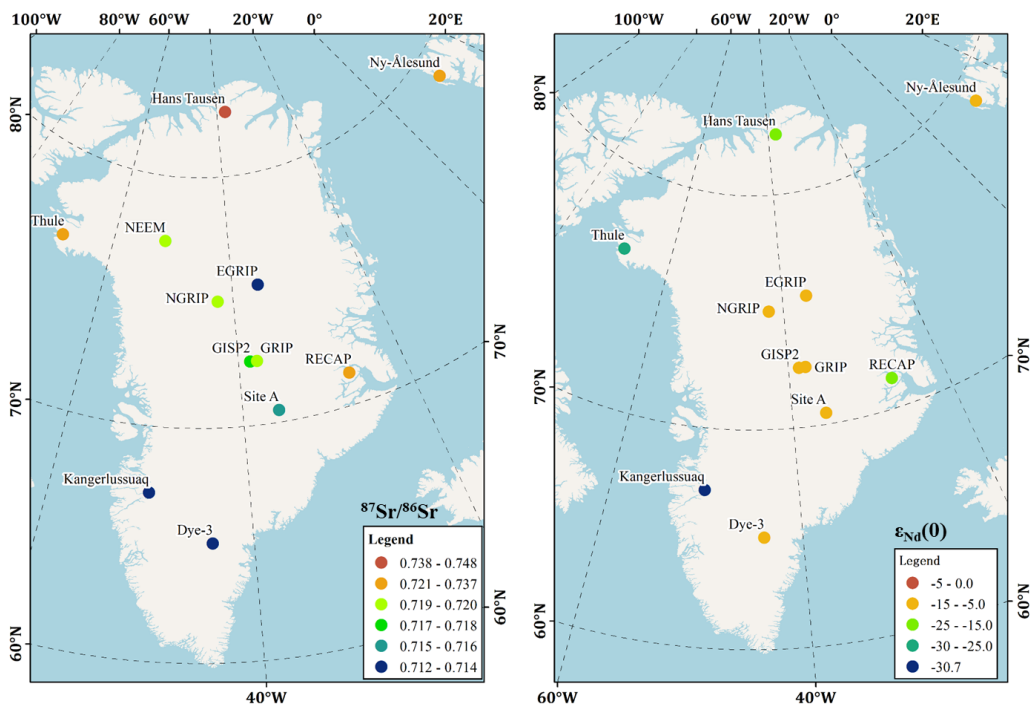
319
 320 Fig. 4. Sampling distribution sites in the Arctic. The types of samples are denoted
 321 with different shapes and colours (Table 3). (AO: Arctic Ocean; BCS: Bering-Chukchi
 322 Sea; BS: Barents Sea; CAA: Canadian Arctic Archipelago; ESS: East Siberian Sea;
 323 KS: Kara Sea; LS: Laptev Sea; SV: Svalbard) (this figure was created with ArcGIS).

324 **3.2.1 Sr-Nd data from snow/ice and sand samples of the Greenland ice sheet**

325 Sr-Nd data from the East Greenland Ice Core Project (EGRIP) and the North
326 GRIP (NGRIP) were measured via snowpits. Sr-Nd data were also measured in GRIP,
327 GISP2 and NEEM ice cores, and Renland, Site A, Hans Tausen and Dye 3 shallow ice
328 cores. Sr-Nd data exhibit large differences in these samples (Fig. 5). The Sr-Nd data
329 indicated that the dust sources were variable and showed complicated dust sources in
330 the same location for NGRIP snow (Bory et al., 2002; Bory et al., 2003b). As much
331 more Sr-Nd data from the sand, soil, cryoconite, moraine, and englacial dust samples
332 in the periphery of the GrIS were recently measured (Nagatsuka et al., 2016), $^{87}\text{Sr}/^{86}\text{Sr}$
333 values are high and the $\epsilon_{\text{Nd}}(0)$ values are the least radiogenic in these samples (Table
334 3). Compared with Sr data in NGRIP and EGRIP snowpits (Bory et al., 2002; Bory et
335 al., 2003b), much larger variations were observed for $^{87}\text{Sr}/^{86}\text{Sr}$ in the EGRIP snowpit,
336 and relatively lower $^{87}\text{Sr}/^{86}\text{Sr}$ values were observed in the NGRIP snowpit. The $\epsilon_{\text{Nd}}(0)$
337 values in the interior of the GrIS are relatively consistent, while the large differences
338 are observed at the periphery of the GrIS. Therefore, although the Sr-Nd isotope ratios
339 indicated that Asian deserts might be the main dust source for the GrIS, the ice-free
340 region around the GrIS might be another source for the interior GrIS. Sr-Nd data in
341 sediment samples collected from the Scoresby Sund region by Simonsen et al. (2019)
342 are as follows: the $^{87}\text{Sr}/^{86}\text{Sr}$ ratios range from 0.709689 to 0.736137, and the $\epsilon_{\text{Nd}}(0)$
343 values range from -15.7 to -10.1. Combining Sr-Nd values in snow (Renland, Site A,
344 Hans Tausen and Dye 3) and Dye 3 shallow ice core samples, as proposed by Lupker
345 et al. (2010), the local dust sources may contribute some of the dust to the inland
346 regions and the Sahara is also the most likely additional PSA. The local dust for the
347 free ice of the GrIS may have been neglected in previous studies.

348 The mainstream view of the provenance of dust in inland Greenland deep ice
349 cores (GISP2 and GRIP) is that the dust is from the eastern Asian deserts (the Gobi

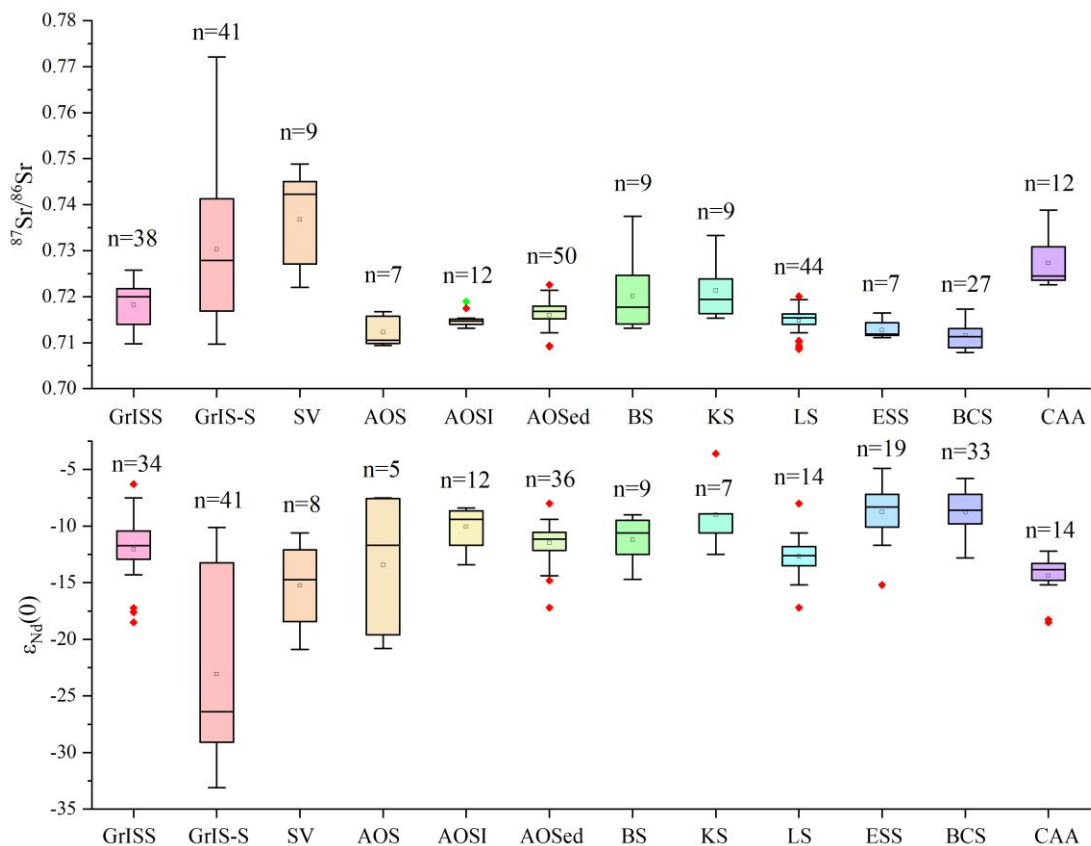
350 and Taklimakan Deserts) based on the best Sr-Nd data matches during the last glacial
 351 period (Biscaye et al., 1997; Svensson et al., 2000; Újvári et al., 2015).
 352 High-resolution Sr isotope data from the Greenland NEEM ice core suggested that
 353 there was a significant Saharan dust influence in Greenland during the last glacial
 354 period (Han et al., 2018). The Sr-Nd data ($>5 \mu\text{m}$) in Holocene RECAP ice core
 355 samples are attributed to proximal dust sources; however, the resolution of the data is
 356 approximately one thousand years (Simonsen et al., 2019). However, the Sr-Nd data
 357 in Greenland deep ice core samples (Biscaye et al., 1997; Svensson et al., 2000),
 358 which have low resolutions and represent multiyear averages with no seasonal or
 359 interannual variations (60 to 200 cm or 30-150 years), need to be considered when
 360 using some data.



361
 362 Fig. 5. $^{87}\text{Sr}/^{86}\text{Sr}$ and $\epsilon_{\text{Nd}}(0)$ data in snow or ice cores, and sand/soil samples from
 363 Ny-Ålesund, Svalbard and GrIS (this figure was created with ArcGIS).

364 **3.2.2 Sr-Nd data from snow and sediment samples in the Arctic Ocean**

365 Surface aeolian dust from mid- or high-latitude continental weathering and arid
 366 deserts may be the most important dust contributor to snow and ice cores. The
 367 $^{87}\text{Sr}/^{86}\text{Sr}$ values are higher and $\epsilon_{\text{Nd}}(0)$ values are lower in snow and sand samples from
 368 Ny-Ålesund, Svalbard (SV) (not including data from Iceland in Fig. 6). The Sr-Nd
 369 data in snow samples from sea ice were measured in bulk, and four of these samples
 370 were collected near the North Pole in the western AO by MOSAIC (October 2020) in
 371 this study (Figs. 4 and 6). The $\epsilon_{\text{Nd}}(0)$ data have much more negative $\epsilon_{\text{Nd}}(0)$ values
 372 (-20.8 to -19.6), which cannot be explained by low latitude potential dust sources. As
 373 shown in Fig. 6, the lowest ϵ_{Nd} values were observed along the ice-free periphery of
 374 the GrIS and SV; therefore, these ice-free regions are potential dust sources for natural
 375 dust in the AO.



376
 377 Fig. 6. Box plot for the Sr-Nd isotopic signatures of the Arctic, including the 12
 378 sub-region samples of snow, sand, soil, sediment from sea ice and sediment cores in

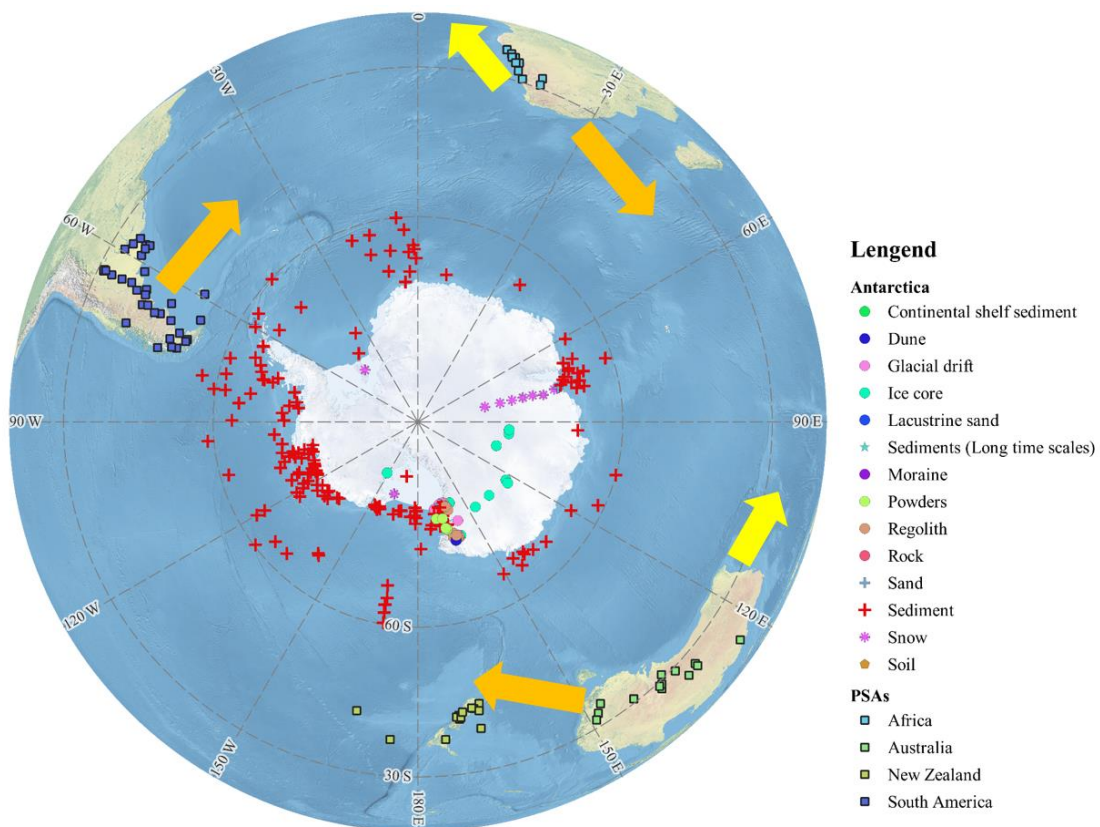
379 dataset (the number of samples for each sub-region are presented (n>5)). (GrIS:
380 Greenland ice sheet (snow samples); GrIS-S: Greenland ice sheet (sand); SV:
381 Svalbard (snow and sand); AOS: Arctic Ocean (sediment); AOSI: Arctic Ocean (sea
382 ice sediment)).

383 The terrigenous material from the Arctic margin sea, including BS, KS, LS, ESS,
384 BCS and CAA, was transported and deposited into the AO, which may be the primary
385 material source for marine sediment. The Sr-Nd data from Arctic surface sediments
386 were based on the literature (Fig. 6), and most samples were sieved at < 45 or 63 μm
387 for bulk. These samples were chosen at the surface or 0-10 cm from the top to better
388 represent the characteristics of coastal terrestrial sources as presented by Maccali et al.
389 (2018). The Sr-Nd values from the sediment samples (including sea ice sediment) are
390 almost the same as those of snow samples from the AO, indicating that the same PSAs
391 exist in the central AO. The Sr-Nd signals in sediment from the AO seem to be close
392 to the BS, KS and LS values, which may contribute to the Transpolar Drift originating
393 from the Siberian shelves and crossing the AO towards the Fram Strait. The sample
394 spatial coverage in each sub-region is variable, and Fig. 6 shows the distinguishing
395 characteristics for each region, but Sr-Nd isotopic values overlap for close
396 geographical regions to the greatest extent. Therefore, these data should be carefully
397 used in the different regions.

398 **3.3. Information on Sr-Nd data from the SH and Antarctic ice sheet**

399 By integrating the literature and adding data with new evidence, dust
400 provenances of low-elevation areas on the periphery of the AIS in the Holocene
401 (including modern) were discussed. The dataset provides a comprehensive overview
402 of the state of knowledge of dust sources and sinks in different sectors of the AIS and
403 PSAs in the SH. The location Sr-Nd datasets from different sectors of Antarctica and

404 AIS are presented in Fig. 7. Sr-Nd data from Antarctica are not evenly distributed, and
 405 more data were measured in western Antarctica and the Ross Sea. Sr-Nd data in PSAs
 406 from the SH (Australia, southern South America (hereafter SSA) and southern Africa
 407 (SA)) clearly showed characteristics in these regions and provided insight for tracing
 408 dust source–sink paths. For example, $^{87}\text{Sr}/^{86}\text{Sr}$ ratios in Australian dust samples range
 409 from 0.709 to 0.732, and $\epsilon_{\text{Nd}}(0)$ values are between -15 and -3 (Revel-Rolland et al.,
 410 2006). Sr-Nd data in Patagonia (39–52 °S) of SSA with more radiogenic Nd (-1–1 for
 411 $\epsilon_{\text{Nd}}(0)$) (Gaiero, 2007). The aeolian dust from Argentina and Chile is confined to the
 412 ranges of $0.7045 < ^{87}\text{Sr}/^{86}\text{Sr} < 0.7130$ and $-5 < \epsilon_{\text{Nd}}(0) < 3$ (Delmonte et al., 2003). The
 413 $^{87}\text{Sr}/^{86}\text{Sr}$ ratios in the sand samples from SA varied between 0.712348 and 0.74716,
 414 and the $\epsilon_{\text{Nd}}(0)$ ratios varied between -24.5 and -8.4 (Delmonte et al., 2003; Gili et al.,
 415 2021). These Sr-Nd data can very clearly distinguish geographic subgroups for PSAs
 416 in SH.



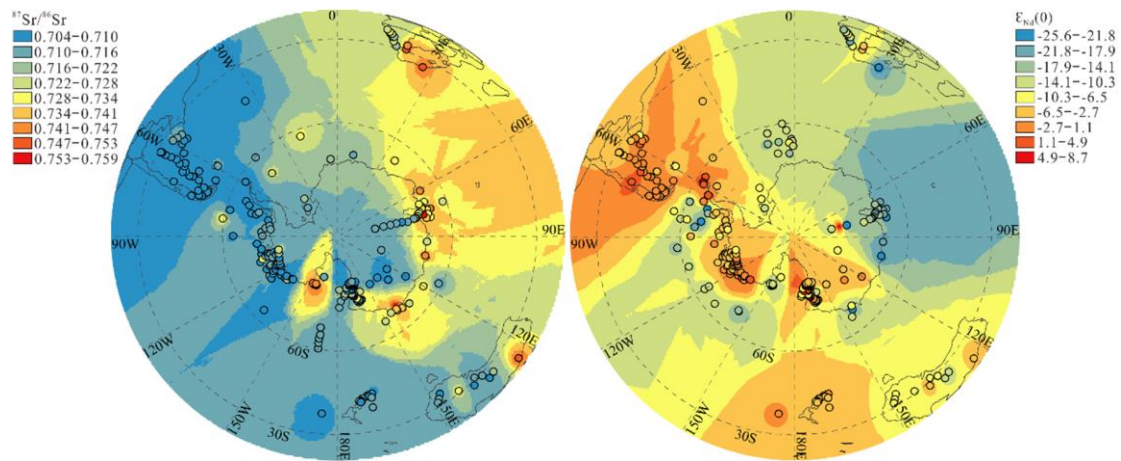
417

418 Fig. 7. The locations of the samples were marked in this database for Sr-Nd isotope

419 ratios from Antarctica and PSAs. The dust transport paths are marked with yellow
420 arrows based on previous studies (Gaiero, 2007; Shao et al., 2010; Gili et al., 2021)
421 (this figure was created with ArcGIS).

422 **3.3.1 Sr-Nd data of sediment in Antarctica**

423 Sr-Nd data for the marine sediment (near-core-top samples) from the
424 Circum-Antarctica, terrigenous materials (aeolian dust, glacial drift and dust in ice
425 core) from the AIS are presented in Fig. 8. The ages of these samples were limited to
426 the Holocene. We compared these data with PSA samples from SH. At some sites, if
427 the samples are >2 , we obtained the average Sr-Nd values in this map. For example,
428 for the Pacific sector (146.78 °E-67.27 °W), $^{87}\text{Sr}/^{86}\text{Sr}$ values ranged from 0.705281 to
429 0.725643; $^{87}\text{Sr}/^{86}\text{Sr}$ values ranged from 0.710616 to 0.738862 for the Indian Ocean
430 sector (20.00 °E-146.78 °E); $^{87}\text{Sr}/^{86}\text{Sr}$ values ranged from 0.715989 to 0.741609 for the
431 Atlantic sector (67.27 °W-20.00 °E) (Hemming et al., 2007). Viewed from Fig. 8, Sr
432 and Nd contours were determined by inverse distance weighted interpolation, and the
433 numbers of data were >2 in some sites, the averages of surface samples were obtained,
434 the patterns of the two isotopic compositions are consistent in all AIS. Although
435 $^{87}\text{Sr}/^{86}\text{Sr}$ values differ between sediments from the Circum-Antarctica and sand of
436 PSAs (Australia, SSA and SA), the $^{87}\text{Sr}/^{86}\text{Sr}$ and $\epsilon_{\text{Nd}}(0)$ patterns from the Pacific
437 sector and Indian Ocean sector are relatively consistent with SSA and SA, which can
438 partly explain the aeolian dust contributing to the entire SO. It seems to be abnormal
439 Sr-Nd values that were found in the Ross Sea and Amundsen Sea, which may have
440 contributed to many more sample numbers in the two regions.



441

442 Fig. 8. Sr versus Nd isotopic compositions for Holocene samples (black circles) at the
 443 AIS and its periphery in ice-free areas, and aeolian dust samples (surface samples
 444 with no accurate ages) from PSAs in Australia, southern Africa and South America
 445 defined by colours, which were determined by inverse distance weighted interpolation
 446 using ArcGIS.

447 3.3.2 Sr-Nd data on the periphery and interior of the Antarctic ice sheet

448 New Sr-Nd data from coastal and low-elevation sites were measured in ice-free
 449 areas near the Filchner–Ronne Ice Shelf, Ross Ice Shelf and Amery Ice Shelf (Fig. 7).
 450 Sr-Nd isotope compositions of four sand samples from southern King George Island
 451 (South Shetland Islands) in West Antarctica, with less radiogenic $^{87}\text{Sr}/^{86}\text{Sr}$ values
 452 ranging from ~ 0.703907 to ~ 0.704157 and relatively higher $\epsilon_{\text{Nd}}(0)$ values ranging
 453 from 4.6 to 6.4. The $^{87}\text{Sr}/^{86}\text{Sr}$ ratios ranged from 0.71135 to 0.72377, and the $\epsilon_{\text{Nd}}(0)$
 454 composition ranged from -13.3 to -9.6 from ice-free areas of Inexpressible Island in
 455 the Ross Sea, West Antarctica. Based on the Sr-Nd data on our own and the literature
 456 (Table 3), we can observe the highest $\epsilon_{\text{Nd}}(0)$ value of > -5.0 in McMurdo and King
 457 George Island. The large variations in $^{87}\text{Sr}/^{86}\text{Sr}$ values and moderate $\epsilon_{\text{Nd}}(0)$ values for
 458 Victoria Land and Ross Sea (including Inexpressible Island). The high $^{87}\text{Sr}/^{86}\text{Sr}$ ratios
 459 and low $\epsilon_{\text{Nd}}(0)$ values for the Amery Ice Shelf have the lowest $\epsilon_{\text{Nd}}(0)$ values of < -15 .
 460 These sub-regions are very close to $\epsilon_{\text{Nd}}(0)$ data from the different sectors of

461 circumpolar sediments (Roy et al., 2007). Therefore, the dataset will be useful for
462 tracing the dust sources or sinks in SO or AIS.

463 However, among these regions, Sr-Nd data have significant differences in some
464 of the endmembers, which are similar, and care must be taken when directly
465 comparing these data to precisely explain the observed isotopic compositions in ice
466 core records. For example, there is overlap of the Sr and Nd isotopic compositions of
467 King George Island, SSA (Patagonia) and McMurdo dry valleys. Sr-Nd data from
468 Inexpressible Island also overlap with the other endmembers (SA, New South Wales
469 and Prydz Bay). Therefore, dust from low-latitude regions (New South Wales and SA)
470 cannot be excluded from East Antarctica (Du et al., 2018; Gili et al., 2021). Another
471 example is the characteristics of snow layers at the Berkner Island ice sheet in western
472 Antarctica. These data can be partly explained by the surface sediment samples from
473 the Weddell Sea sector, with $\epsilon_{Nd}(0)$ values ranging from -10 to -8 (Hemming et al.,
474 2007). Therefore, the dataset from the SH and AIS demonstrates that multiple mixed
475 sources can be inferred for Antarctic surface snow samples. However, among the data
476 from the entire AIS, Sr-Nd isotopic components were measured in only 29 snow
477 samples, and there is an urgent need to collect more data in the future.

478 Information on Sr-Nd data in Antarctic ice cores during the Holocene and
479 glacial-interglacial times is presented by integrating the literature (Du et al., 2022). To
480 obtain enough dust particles, the different age interval samples were merged. For
481 example, each sample represents approximately 40-160 years for the Vostok ice core,
482 which is a few thousand years to obtain a single large-volume sample (Delmonte et al.,
483 2008). Alternatively, several ice core sections from different depths were integrated to
484 obtain a few large samples for the Sr and Nd isotope analyses of the Talos Dome ice
485 core (Delmonte et al., 2010b). A relatively high resolution (spanning between ~ 3 and

486 ~ 30 yrs.) was used in the Taylor Dome ice core (Aarons et al., 2016). Sr-Nd data in
487 the Antarctica deep ice core mainly focus on the coastal and inland areas of the EAIS.
488 As previously mentioned, the dust source is similar to that of the modern samples in
489 the Dome C and Vostok ice cores during the Holocene and interglacial periods, which
490 can be explained by an SSA provenance; an additional hypothesis explains the
491 isotopic signature of Holocene dust in central East Antarctica (Delmonte et al., 2008,
492 Delmonte et al., 2019). Sr-Nd data in the Talos Dome, Taylor Dome and Taylor
493 Glacier ice cores during the Holocene point towards a local dust provenance
494 (Delmonte et al., 2019; Aarons et al., 2016, 2017). Therefore, the Sr and Nd data from
495 East Antarctica ice cores during the Holocene and interglacial periods indicate a
496 well-mixed atmospheric background involving a mixture of two or more sources in
497 the SH (Fig. 8). The study demonstrated that SA emerges as the second most
498 important dust source to East Antarctica during interglacial periods (Gili et al., 2021).

499 However, the glacial stage (stage 4: ~ 60 ka and stage 6: ~ 160 ka) samples in the
500 Vostok ice core span a very narrow range of Sr compositions ($0.708219 < {}^{87}\text{Sr}/{}^{86}\text{Sr} <$
501 0.708452) and Nd compositions ($1.1 < \epsilon_{\text{Nd}}(0) < 5.0$), which can also be explained by
502 the Sr-Nd data in sand samples from southern King George Island (${}^{87}\text{Sr}/{}^{86}\text{Sr}$ values
503 ranging from ~0.703907 to ~0.704157 and $\epsilon_{\text{Nd}}(0)$ values ranging from 4.6 to 6.4).
504 The ${}^{87}\text{Sr}/{}^{86}\text{Sr}$ and $\epsilon_{\text{Nd}}(0)$ isotopic compositions of dust in the Taylor Glacier ice core
505 samples during the last glacial period indicated that dust may originate from SSA and
506 from potential local source areas in the Ross Sea Sector (Delmonte et al., 2010b;
507 Aarons et al., 2016; Aarons et al., 2017). Therefore, these data suggest that the
508 glacial-period dust in East Antarctic ice cores also contributes from local
509 contributions. However, almost no Sr-Nd data were obtained from West Antarctic
510 deep ice cores, which limits our understanding of the dust transport in the spatial and

511 temporal distribution of the entire AIS. More importantly, the ages of Sr-Nd data in
512 surface aeolian dust from the AIS and PSAs from SH are unknown, which is limited
513 to accurate dust source or sink tracing.

514 **4. Data availability**

515 All datasets and the associated metadata table presented in this study are
516 available through a Big Earth Data Platform for Three Poles. The dataset can be
517 downloaded from <https://doi.org/10.11888/Cryos.tpd.c.272100> (Du et al., 2022). In
518 this repository, all datasets are provided in Excel spreadsheet format together with
519 metadata files.

520 **5. Conclusions**

521 The maintenance integrated Sr-Nd dataset was presented from the remote three
522 poles, and these data are not easily collected because of the extremely cold and high
523 altitude environment. The dataset is complicated and includes snow, sand, soil, loess,
524 deposits, sediment and other types. We presented case studies of snow, ice core and
525 sediment are intended to demonstrate the Sr-Nd characteristics in the Third Pole
526 glaciers or Arctic and Antarctica ice sheets. These integrated data can provide a new
527 perspective into present and paleodust sources or sinks from the three poles, more
528 importantly, which clearly emphasizes the following points for potential users of the
529 datasets provided with this paper:

- 530 1. This Sr-Nd dataset enables us to map the standardized locations in the remote
531 three poles, while the use of sorting criteria related to the sample location, type or
532 resolution permits us to trace the dust sources or sinks based on their isotopic
533 signatures.
- 534 2. For the third pole, each sub-region of Sr-Nd data was provided, the integration of
535 these data between sand (soil) and snow samples for six sub-regions allowed us to

536 clearly understand the Sr-Nd data characteristics in the Third Pole. The data will
537 be useful for tracing the local or long-distance transported dust of the source and
538 sink for user.

539 3. The Sr-Nd characteristics in snow (ice) and sediment samples showed that there
540 are significant differences in different sub-regions for the entire Arctic, which
541 would be useful for tracing dust sources or sinks

542 4. The new data from Arctic and Antarctic samples emphasized the ice-free regions
543 on the periphery of the ice sheets, which may be important local dust sources.
544 However, in particular, Sr-Nd data overlap with the low-latitude regions in
545 Antarctica, the paucity of data in Antarctica is serious and future studies should
546 concentrate on this aspect.

547 **Author contributions.** CX, ZD, and SA designed the study, ZD, JY, CX and SA
548 wrote the manuscript. ZD, LW, NW, SW, YL collected the samples in the field and
549 produced the data. ZD, NW, LW, SW, YL, ZW, and XM performed the analysis. All
550 authors contributed to the final form of the manuscript.

551 **Competing interests.** The authors declare that they have no conflicts of interest.
552 This work was supported by the Strategic Priority Research Program of the Chinese
553 Academy of Sciences (XAD19070103), the National Natural Science Foundation of
554 China (Grant Nos. 42071086 and 41971088), the Youth Innovation Promotion
555 Association, CAS (2020419) and the State Key Laboratory of Cryospheric Science
556 (SKLCS-ZZ-2022). We thank all people involved in snow samples collecting from
557 central Arctic Ocean by the expedition of the Research Vessel Polarstern for their
558 great logistical supports during MOSAiC in 2019–2020. We also thank the Chinese
559 Arctic and Antarctic Administration contributing to the part of MOSAiC.

560
561

562 **References:**

- 563 Aarons, S., Aciego, S., Gabrielli, P., Delmonte, B., Koornneef, J., Wegner, A., and Blakowski, M.: The
564 impact of glacier retreat from the Ross Sea on local climate: Characterization of mineral dust in the
565 Taylor Dome ice core, East Antarctica, *Earth Planet. Sc. Lett*, 444, 34–44,
566 <https://doi.org/10.1016/j.epsl.2016.03.035>, 2016.
- 567 Aarons, S. M., Aciego, S. M., Arendt, C. A., Blakowski, M. A., Steigmeyer, A., Gabrielli, P.,
568 SierraHernández, M. R., Beaudon, E., Delmonte, B., Baccolo, G., May, N. W., and Pratt, K. A.: Dust
569 composition changes from Taylor Glacier (East Antarctica) during the last glacial-interglacial transition:
570 A multi-proxy approach, *Quat. Sci. Rev*, 162, 60-71, <https://doi.org/10.1016/j.quascirev.2017.03.011>,
571 2017.
- 572 Abbott, A. N., Lühr, S. C., Payne, A., Kumar, H., and Du, J.: Widespread lithogenic control of marine
573 authigenic neodymium isotope records? Implications for paleoceanographic reconstructions.
574 *Geochimica et Cosmochimica Acta*, 319, 318-336. <https://doi.org/10.1016/j.gca.2021.11.021>.
- 575 Asahara, Y., Takeuchi, F., Nagashima, K., Harada, N., Yamamoto, K., Oguri, K., Tadai, O.: Provenance
576 of terrigenous detritus of the surface sediments in the Bering and Chukchi Seas as derived from Sr and
577 Nd isotopes: implications for recent climate change in the Arctic regions. *Deep Sea Res. Part II* 61–64,
578 155–171. <https://doi.org/10.1016/j.dsr2.2011.12.004>, 2012.
- 579 Bayon, G., German, C.R., Boella, R.M., Milton, J.A., Taylor, R.N., Nesbitt, R.W.: An improved method
580 for extracting marine sediment fractions and its application to Sr and Nd isotopic analysis. *Chem. Geol.*
581 187, 179-199. [https://doi.org/10.1016/S0009-2541\(01\)00416-8](https://doi.org/10.1016/S0009-2541(01)00416-8), 2002.
- 582 Bayon, G., Freslon, N., Germain, Y., Bindeman, I.N., Trinquier, A., Barrat, J.A.: A global survey of
583 radiogenic strontium isotopes in river sediments. *Chem. Geol.* 559, 119958.
584 <https://doi.org/10.1016/j.epsl.2022.117490>, 2021.
- 585 Biscaye, P.E., Grousset, F.E., Revel, M., Van der Gaast, S., Zielinski, G.A., Vaars, A., and Kukla, G.:
586 Asian provenance of glacial dust (stage 2) in the Greenland Ice Sheet Project 2 ice core, Summit,
587 Greenland. *J. Geophys. Res.-Oceans*, 102, 26765-26781. <https://doi.org/10.1029/97JC01249>, 1997.
- 588 Blakowski, M.A., Aciego, S.M., Delmonte, B., Baroni, C., Salvatore, M.C., Sims, K.W.W.: A
589 Sr–Nd–Hf isotope characterization of dust source areas in Victoria Land and the McMurdo Sound
590 sector of Antarctica. *Quat. Sci. Rev.* 141, 26–37. <https://doi.org/10.1016/j.quascirev.2016.03.023>.
- 591 Blanchet C L.: A database of marine and terrestrial radiogenic Nd and Sr isotopes for tracing
592 earth-surface processes. *Earth Syst. Sci. Data*, 11(2):741-759. <https://doi.org/10.5194/essd-11-741-2019>,
593 2019.
- 594 Bory, J. M., Biscaye, P. E., Svensson, A., and Grousset, F. E.: Seasonal variability in the origin of
595 recent atmospheric mineral dust at NorthGRIP, Greenland. *Earth Planet. Sc. Lett*, 196(3-4):123-134.
596 [https://doi.org/10.1016/S0012-821X\(01\)00609-4](https://doi.org/10.1016/S0012-821X(01)00609-4), 2002.
- 597 Bory, A.M., Biscaye, P.E., Piotrowski, A.M., Steffensen, J.P.: Regional variability of ice core dust
598 composition and provenance in Greenland. *Geochem. Geophys. Geosy*, 4.
599 <https://doi.org/10.1029/2003GC000627>, 2003a.
- 600 Bory, A.J.M., Biscaye, P.E., Grousset, F.E.: Two distinct seasonal Asian source regions for mineral dust
601 deposited in Greenland (NorthGRIP). *Earth Sci. Rev.* 30. <https://doi.org/10.1029/2002GL016446>,
602 2003b.
- 603 Bory, A., Wolff, E., Mulvaney, R., Jagoutz, E., Wegner, A., Ruth, U., and Elderfield, H.: Multiple
604 sources supply eolian mineral dust to the atlantic sector of coastal antarctica: evidence from recent
605 snow layers at the top of Berkner island ice sheet, *Earth Planet. Sci. Lett*, 291(1-4), 138-148,

606 <https://doi:10.1016/j.epsl.2010.01.006>, 2010.

607 Chen, J., Li, G., Yang, J., Rao, W., Lu, H., Balsam, W., Sun, Y., and Ji, J.: Nd and Sr isotopic
608 characteristics of Chinese deserts: implications for the provenances of Asian dust. *Geochimica Et*
609 *Cosmochimica Acta*, 71, 3904-3914, <https://doi.org/10.1016/j.gca.2007.04.033>, 2007.

610 Delmonte, B., Quaternary variations and origin of continental dust in East Antarctica, PhD Thesis,
611 Université degli Studi di Siena / Université Joseph Fourier - Grenoble 1, 2003.

612 Delmonte, B., Andersson, P.S., Hansson, M., Schoberg, H., Petit, J.R., Basile-Doelsch, I., and Maggi,
613 V.: Aeolian dust in East Antarctica (EPICA-Dome C and Vostok): provenance during glacial ages over
614 the last 800 kyr. *Geophys. Res. Lett.*, 35 (7), L07703, <https://doi:10.1029/2008GL033382>, 2008.

615 Delmonte, B., Andersson, P.S., Schoberg, H., Hansson, M., Petit, J.R., Delmas, R., Gaiero, D.M.,
616 Maggi, V., and Frezzotti, M.: Geographic provenance of Aeolian dust in East Antarctica during
617 Pleistocene glaciations: preliminary results from Talos Dome and comparison with East Antarctic and
618 new Andean ice core data. *Quat. Sci. Rev.*, 29, 256–264, <https://doi.org/10.1016/j.quascirev.2009.05.010>,
619 2010a.

620 Delmonte, B., Baroni, C., Andersson, P.S., Schöberg, H., Hansson, M., Aciego, S., Petit, J.-R., Albani,
621 S., Mazzola, C., Maggi, V., and Frezzotti, M.: Aeolian dust in the Talos Dome ice core (East Antarctica,
622 Pacific/Ross Sea sector): Victoria Land versus remote sources over the last two climate cycles. *J. Quat.*
623 *Sci.*, 25 (8), 1327–1337, <https://doi.org/10.1002/jqs.1418>, 2010b.

624 Delmonte, B., Baroni, C., Andersson, P. S., Narcisi, B., Salvatore, M. C., Petit, J. R., Scarchilli, C.,
625 Frezzotti, M., Albani, S., and Maggi, V.: Modern and Holocene aeolian dust variability from Talos
626 Dome (Northern Victoria Land) to the interior of the Antarctic ice sheet, *Quaternary Sci. Rev.*, 64,
627 76–89, doi:10.1016/j.quascirev.2012.11.033, 2013.

628 Delmonte, B., Paleari, C. I., Andò S., Garzanti, E., Andersson, P. S., Petit, J. R., Crosta, X., Narcisi, B.,
629 Baroni, C., Salvatore, M., Baccolo, G., and Maggi.: Causes of dust size variability in central East
630 Antarctica (Dome B): Atmospheric transport from expanded South American sources during Marine
631 Isotope Stage 2. *Quaternary Sci. Rev.*, 168, 55–68, <https://doi.org/10.1016/j.quascirev.2017.05.009>,
632 2017.

651 Delmonte, B., Winton, H., Baroni, M., Baccolo, G., Hansson, M., Andersson, P., Baroni, C., Salvatore,
652 M., Lanci, L., and Maggi, V.: Holocene dust in East Antarctica: provenance and variability in time and
653 space. *Holocene*, 30 (4), 546-558, <https://doi.org/10.1177/0959683619875188>, 2019.

654 Dong, Z., Shao, Y., Qin, D., Kang, S., Wei, W., Wang, X., and Wang, S.: Hf-Nd-Sr isotopic composition
655 as fingerprint for long-range transported eolian dust deposition in glacier snowpack of eastern Tibetan
656 Plateau. *J. Geophys. Res.*, 123, 7013–7023, <https://doi.org/10.1029/2018JD028581>, 2018.

657 Du, Z., Xiao, C., Liu, Y., Wu, G.: Geochemical characteristics of insoluble dust as a tracer in an ice core
658 from Miaoergou Glacier, east Tien Shan. *Glob. Planet. Chang.*, 127, 12-21.
659 <http://doi.org/10.1016/j.gloplacha.2015.01.011>, 2015.

660 Du, Z., Xiao, C., Ding, M., and Li, C.: Identification of multiple natural and anthropogenic sources of
661 dust in snow from Zhongshan Station to Dome A, East Antarctica. *J. Glaciol.*, 64: 855–865,
662 <https://doi.org/10.1017/jog.2018.72>, 2018.

663 Du, Z., Xiao, C., Wang, Y., Liu, S., and Li, S.: Dust provenance in Pan-third pole modern glacierized
664 regions: What is the regional source?. *Environmental Pollution*, 250(JUL.): 762-772,
665 <https://doi.org/10.1016/j.envpol.2019.04.068>, 2019a.

666 Du, Z., Xiao, C., Dou, T., Li, S., An, H., Liu, S., and Liu K.: Comparison of Sr–Nd–Pb isotopes in
667 insoluble dust between northwestern China and high-latitude regions in the Northern Hemisphere.

668 Atmospheric Environment, 214:116837, <https://doi.org/10.1016/j.atmosenv.2019.116837>, 2019b.

669 Gaiero, D.M., Brunet, F., Probst, J.L., Depetris, P.J.: A uniform isotopic and chemical signature of dust
670 exported from Patagonia: rock sources and occurrence in southern environments. *Chem. Geol.* 238 (1),
671 107-120, <https://doi.org/10.1016/j.chemgeo.2006.11.003>, 2007.

672 Gili, S., Vanderstraeten, A., Chaput, A., King, J., Gaiero, D., Delmonte, B., Vallelonga, P., Formenti, P.,
673 Di Biagio, C., Cazanaou, M. and Pangui, E.: Southern Africa: The Missing Piece To The Dust
674 Provenance Puzzle of East Antarctica? *Communications Earth & Environment*, 2021.

675 Grousset, F. E., Biscaye, P. E., Revel, M., Petit, J., Pye, K., Joussaume, S., and Jouzel, J.: Antarctic
676 (Dome C) ice-core dust at 18 k.y. B. P.: isotopic constraints on origins, *Earth Planet. Sci. Lett.* 111,
677 175–182, [https://doi.org/10.1016/0012-821X\(92\)90177-W](https://doi.org/10.1016/0012-821X(92)90177-W), 1992.

678 Grousset, F. E., Parra, M., Bory, A., Martinez, P., Bertrand, P., Shimmiel, G and Ellam, R. M.: Saharan
679 wind regimes traced by the Sr–Nd isotopic composition of subtropical Atlantic sediments: last glacial
680 maximum vs today, *Quaternary Sci. Rev.* 17, 395–409, [https://doi.org/10.1016/S0277-3791\(97\)00048-6](https://doi.org/10.1016/S0277-3791(97)00048-6),
681 1998.

682 Han, C., Hur, S. D., Han, Y., Lee, K., Hong, S., Erhardt, T., Fischer, H., Svensson, A., Steffensen, JP.,
683 and Vallelonga, P.: High-resolution isotopic evidence for a potential Saharan provenance of Greenland
684 glacial dust. *Sci Rep.* 8, 15582, <https://doi.org/10.1038/s41598-018-33859-0>, 2018.

685 Hemming, S.R., van de Flierdt, T., Goldstein, S.L., Franzese, A.M., Roy, M., Gastineau, G., Landrot, G.:
686 Strontium isotope tracing of terrigenous sediment dispersal in the Antarctic Circumpolar Current:
687 implications for constraining frontal positions. *Geochem. Geophys. Geosyst.* 8 (6), Q06N13,
688 <https://doi:10.1029/2006GC001441>, 2007.

689 Jacobsen, S.B., Wasserburg, G.J. (1980) Sm-Nd evolution of chondrites. *Earth Planet. Sci. Lett.* 50,
690 139-155.

691 Jonell, T.N., Li, Y., Blusztajn, J., Giosan, L., Clift, P.D.: Signal or noise? Isolating grain size effects on
692 Nd and Sr isotope variability in Indus delta sediment provenance. *Chem. Geol.* 485, 56e73.
693 <https://doi.org/10.1016/j.chemgeo.2018.03.036>, 2018.

694 Lambert, F., Kug, J. S., Park, R. J., Mahowald, N., Winckler, G., Abe-Ouchi, A., and Lee, J. H.: The
695 role of mineral-dust aerosols in polar temperature amplification, *Nat. Clim. Change*, 3, 487– 491,
696 <https://doi.org/10.1038/nclimate1785>, 2013.

697 Li, X., Che, T., Li, X., Wang, L., Duan, A., Shangguan, D., Pan, X., Fang, M., and Bao, Q.: CASEarth
698 Poles: Big data for the Three Poles, *B. Am. Meteorol. Soc.*, 101, E1475–E1491, 2020

699 Lin, Y. C., Feng, J. L.: Aeolian dust contribution to the formation of alpine soils at Amdo (Northern
700 Tibetan Plateau). *Geoderma* 259, 104e115. <https://doi.org/10.1016/j.geoderma.2015.05.012>, 2015.

701 Lupker, M., Aciego, S.M., Bourdon, B., Schwander, J., and Stocker, T.F.: Isotopic tracing (Sr, Nd, U and
702 Hf) of continental and marine aerosols in an 18th century section of the Dye-3 ice core (Greenland).
703 *Earth Planet. Sci. Lett.* 295. <http://dx.doi.org/10.1016/j.epsl.2010.04.010>, 2010.

704 Maccali, J., Hillaire-Marcel, C., Not, C.: Radiogenic isotope (Nd, Pb, Sr) signatures of surface and sea
705 ice-transported sediments from the Arctic Ocean under the present interglacial conditions. *Polar
706 Research*, 37(1):1442982, 2018. <https://doi.org/10.1080/17518369.2018.1442982>.

707 Meinhardt, A.K., Pahnke, K., Böning, P., Schnetger, B., Brumsack, H.J.: Climate change and response
708 in bottom water circulation and sediment provenance in the central Arctic Ocean since the last glacial.
709 *Chem. Geol.* 427, 98–108. <http://dx.doi.org/10.1016/j.chemgeo.2016.02.019>, 2016.

710 Nagatsuka, N., Takeuchi, N., Nakano, T., Kokado, E., and Li, Z.: Sr, Nd, and Pb stable isotopes of
711 surface dust on Urumqi glacier No.1 in western China. *Ann. Glaciol.*, 51(56), 95–105.

712 <https://doi.org/10.3189/172756411795931895>, 2010.

713 Nagatsuka, N., Takeuchi, N., Uetake, J., Shimada, R., Onuma, Y., Tanaka, S., and Nakano, T.:
714 Variations in Sr and Nd isotopic ratios of mineral particles in cryoconite in Western Greenland.
715 *Frontiers in Earth Science* 4, 93, <https://doi.org/10.3389/feart.2016.00093>, 2016.

716 Rao, W.B., Yang, J.D., Chen, J., Li, G.L.: Sr–Nd isotope geochemistry of eolian dust of the
717 arid-semiarid areas in China: implications for loess provenance and monsoon evolution. *Chin. Sci. Bull.*
718 51 (12), 1401–1412, 2006. <https://doi.org/10.1007/s11434-006-2008-1>.

719 Revel, M., Sinko, J. A., Grousset, F. E., and Biscaye, P. E.: Sr and Nd isotopes as tracers of North
720 Atlantic lithic particles: Paleoclimatic implications, *Paleoceanography*, 11, 95–113,
721 <https://doi.org/10.1029/95PA03199>, 1996.

722 Revel-Rolland M, De Deckker, P., Delmonte, B., Hesse, P.P., Magee, J.W., Basile-Doelsch, Grousset, F.,
723 and Bosch, D.: Eastern Australia: A possible source of dust in East Antarctica interglacial ice. *Earth*
724 *Planet. Sc. Lett.* 249(1–2): 1–13, <https://doi.org/10.1016/j.epsl.2006.06.028>, 2006.

725 Robinson, S., Ivanovic, R., Flierdt, T. Van De, Blanchet, L., Tachikawa, K., Martin, E.E., Falco, C.P.C.,
726 Williams, T., Gregoire, L., Plancherel, Y., Jeandel, C., Arsouze, T.: Global continental and marine
727 detrital ϵNd : an updated compilation for use in understanding marine Nd cycling. *Chem. Geol.* 567,
728 120119. <https://doi.org/10.1016/j.chemgeo.2021.120119>, 2021.

729 Roy, M., van de Flierdt, T., Hemming, S. R., and Goldstein, S. L.: $^{40}\text{Ar}/^{39}\text{Ar}$ ages of hornblende grains
730 and bulk Sm/Nd isotopes of circum-Antarctic glacio-marine sediments: Implications for sediment
731 provenance in the southern ocean, *Chem. Geol.*, 244, 507–519,
732 <https://doi.org/10.1016/j.chemgeo.2007.07.017>, 2007.

733 Shao, Y., Wyrwoll, K.H., Chappell, A., Huang, J., Lin, Z., McTainsh, G.H., Yoon, S.: Dust cycle: an
734 emerging core theme in Earth system science. *Aeolian Res.* 2 (4), 181–204.
735 <https://doi.org/10.1016/j.aeolia.2011.02.001>, 2011.

736 Simonsen, M. F., Baccolo, G., Blunier, T., Borunda, A., Delmonte, B., Frei, R., Goldstein, S., Grinsted,
737 A., Kjær, A.A., Sowers, T., Svensson, A., Vinther, B., Vladimirova, D., Winckler, G., Winstrup, M., and
738 Vallelonga, P.: East Greenland ice core dust record reveals timing of Greenland ice sheet advance and
739 retreat. *Nature Communications*, 10(1):1-8, <https://doi.org/10.1038/s41467-019-12546-2>, 2019.

740 Skiles, S.M., Flanner, M., Cook, J.M. Dumont, M., Painter, T. H.: Radiative forcing by light-absorbing
741 particles in snow. *Nature Clim Change* 8, 964–971. <https://doi.org/10.1038/s41558-018-0296-5>, 2018.

742 Struve, T., Pahnke, K., Lamy, F., Wengler, M., Bönning, P., Winckler, G.: A circumpolar dust conveyor in
743 the glacial Southern Ocean. *Nature Communications*, 11(1), 1–11.
744 <https://doi.org/10.1038/s41467-020-18858-y>, 2020.

745 Svensson, A., Biscaye, P.E., Grousset, F.E.: Characterization of late glacial continental dust in the
746 Greenland Ice Core Project ice core. *J. Geophys. Res.: Atmosphere*, 105, 4637–4656,
747 <https://doi.org/10.1029/1999JD901093>, 2000.

748 Tüken, T., Eisenhauer, A., Wiegand, B., Hansen, B.T., 2002. Glacial–interglacial cycles in Sr and Nd
749 isotopic composition of Arctic marine sediments triggered by Svalbard/Barents Sea ice sheet. *Marien*
750 *Geology* 182, 351–372. [https://doi.org/10.1016/S0025-3227\(01\)00248-1](https://doi.org/10.1016/S0025-3227(01)00248-1).

751 Újvári, G., Stevens, T., Svensson, A., Klötzli, U.S., Manning, C., Németh, T., Kovács, J., Sweeney,
752 M.R., Gocke, M., Wiesenberg, G.L.B., Markovic, S.B., Zech, M.: Two possible source regions for
753 central Greenland last glacial dust. *Geophys. Res. Lett.* 42, 10,399–310, 408,
754 <https://doi.org/10.1002/2015GL066153>, 2015.

755 Walter, H.J., Hegner, E., Diekmann, B., Kuhn, G., van der Loeff, M.M.R.: Provenance and transport of

756 terrigenous sediment in the South Atlantic Ocean and their relations to glacial and interglacial cycles:
757 Nd and Sr isotopic evidence. *Geochimica Et Cosmochimica Acta* 64 (22), 3813–3827.
758 [https://doi.org/10.1016/S0016-7037\(00\)00476-2](https://doi.org/10.1016/S0016-7037(00)00476-2), 2000.

759 Wei, T., Dong, Z., Kang, S., Qin, X., Guo, Z.: Geochemical evidence for sources of surface dust
760 deposited on the Laohugou glacier, Qilian Mountains. *Appl. Geochem.* 79, 1-8.
761 <http://doi.org/10.1016/j.apgeochem.2017.01.024>, 2017.

762 Wei, T., Dong, Z., Kang, S., Rostami, M., Ulbrich, S., and Shao, Y.: Hf-Nd-Sr isotopic fingerprinting
763 for aeolian dust deposited on glaciers in the northeastern Tibetan Plateau region. *Glob. Planet. Chang.*
764 177, 69–80, <https://doi.org/10.1016/j.gloplacha.2019.03.015>, 2019.

765 Wei, T., Brahney, J., Dong, Z., Kang, S., Zong, C., Guo, J., Yang, Lin., Qin, X.: Hf-Nd-Sr Isotopic
766 Composition of the Tibetan Plateau Dust as a Fingerprint for Regional to Hemispherical Transport.
767 *Environmental Science & Technology*, 55(14). <https://doi.org/10.1021/acs.est.0c04929>, 2021.

768 Wu, G., Zhang, C., Zhang, X., Tian, L., Yao, T.: Sr and Nd isotopic composition of dust in Dunde ice
769 core, Northern China: implications for source tracing and use as an analogue of long-range transported
770 Asian dust. *Earth Planet. Sci. Lett.*, 299 (3), 409-416. <http://doi.org/10.1016/j.epsl.2010.09.021>, 2010.

771 Xie, Y., Liu, L., Kang, C., Chi, Y.: Sr-Nd isotopic characteristics of the Northeast Sandy Land, China
772 and their implications for tracing sources of regional dust. *Catena* 184, 104303.
773 <https://doi.org/10.1016/j.catena.2019.104303>, 2020.

774 Xu, J., Yu, G., Kang, S., Hou, S., Zhang, Q., Ren, J., Qin, D.: Sr-Nd isotope evidence for modern
775 aeolian dust sources in mountain glaciers of western China. *J. Glaciol.*, 58 (211), 859-865.
776 <http://doi.org/10.3189/2012JG12J006>, 2012.

777 Winton, V. H. L., Edwards, R., Delmonte, B., Ellis, A., Andersson, P. S., Bowie, A., Bertler, N. A. N.,
778 Neff, P., and Tuohy, A.: Multiple sources of soluble atmospheric iron to Antarctic waters, *Global*
779 *Biogeochem. Cy.*, 30, 421–437, <https://doi.org/10.1002/2015GB005265>, 2016.

780
781
782
783
784
785
786
787
788
789
790
791
792
793
794
795
796
797
798
799

Table 1. Data distribution locations and sample types for $^{87}\text{Sr}/^{86}\text{Sr}$ and $\epsilon_{\text{Nd}}(0)$ from 89 references.

Region	Characteristics	Data characteristics	Attribution/ harmonization of coordinates	Attribution sorting of criteria	Number of data points
Third Pole					485
Kunnun Mountain (Pamirs)	Peer-reviewed publications	Snow, River Sediment, Moraine	Yes	Yes	39
Tibet Plateau	Peer-reviewed publications and own research articles	Snow, Soil, Sand, River Sediment	Yes	Yes	102
Himalaya Mountain	Peer-reviewed publications	Snow, River Sediment	Yes	Yes	14
Qilian Mountain	Peer-reviewed publications and own research articles	Snow, Ice, River Sediment, Soil, Moraine	Yes	Yes	66
Hengduan Mountain	Peer-reviewed publications	Snow, Soil	Yes	Yes	17
Western Chinese Deserts	Peer-reviewed publications and own research articles	Sand, Dune, Fluvial, Lacustrine, Proluvial	Yes	Yes	219
Chinese Loess Plateau	Peer-reviewed publications and own research articles	Loess	Yes	Yes	21
Others (Qinling and Linxia Basin)	Peer-reviewed publications	River sediment	Yes	Yes	7
Pan-third Pole	Peer-reviewed publications and own research articles	Snow, Ice, Sand, Soil, Loess, Moraine, Lacustrine, Dune	Yes	Yes	250
Arctic					727
Greenland ic sheet	Peer-reviewed publications, own research articles and own measurements	Snow, Ice, Cryoconite, Sand, Sediment, Rock	Yes	Yes	186
Svalbard (Atlantic Ocean)	Peer-reviewed publications and own research articles	Snow, Sand, Sediment	Yes	Yes	32
Arctic Ocean	Peer-reviewed publications, own research articles and own measurements	Snow, Sediment, Waters	Yes	Yes	496
Others (Rivers and Alaska)	Peer-reviewed publications and own research articles	Snow, Soil (Sand), River Sediment	Yes	Yes	13
Antarctica					777
East Antarctica	Peer-reviewed publications and own research articles	Snow, Ice, Sand, Regolith, Glacial drift, Dune, Moraine, Aeolian deposit, Rock, Sediment	Yes	Yes	298
West Antarctica	Peer-reviewed publications and own measurements	Snow, Ice, Sand, Rock, Sediment	Yes	Yes	44
Southern Ocean	Peer-reviewed publications	Sediment	Yes	Yes	435
PSA in Southern Hemisphere					181
South America	Peer-reviewed publications	Loess, Soil, Sediment, Aeolian dust	Yes	Yes	57
Southern Africa	Peer-reviewed publications	Aeolian dust, Loess,	Yes	Yes	53

Sediment deposit, Aerosol						
Australia	Peer-reviewed publications	Sand, Loess, Dune,	Yes	Yes	24	
Lacustrine, Sediment						
New Zealand	Peer-reviewed publications	Loess, Aeolian deposits	Yes	Yes	16	
Others	Peer-reviewed publications	Sediment	Yes	Yes	31	
<hr/>						
Grain sizes	Peer-reviewed publications	Sand, Loess, Sediment,	Yes	Yes	206	
Rock						
Methods	Peer-reviewed publications	Loess, Sand, Cryoconite,	Yes	Yes		
Rock, Moraine, Dust,						
209						
Aerosol, River sediment						
<hr/>						
Grand total					2835	

801

802

803

804

805

806

Table 2. Snow, sand and soil samples were located in the third pole glaciers and PSAs of dust generation. Headers from left to right: Label: the number of glaciers; Sub-regions; Glacier name; Site name: name of the sampling site where the samples were taken; Longitude and Latitude; sampling location; Sample type: Snow, sand or soil; Elevation: m a.s.l; Isotopic ratios of Sr and $\epsilon_{\text{Nd}}(0)$; Ref.: reference publications. The different colours represent different sub-regions.

Label	Glacier name	Sub-regions	Latitude (° N)	Longitude (° E)	Mountains	Sample type	Elevation (m a.s.l)	$^{86}\text{Sr}/^{87}\text{Sr}$	$\epsilon_{\text{Nd}}(0)$	Ref
1	Musidao	Region I	47.10	85.55	Altai	Snow	3605	0.713185–0.713571	-6.55–-4.80	Xu et al., 2012
2	Muztagata		38.28	75.10	East Pamirs	Snow	6365	0.717187–0.717415	-10.3–-8.4	Xu et al., 2012
3	Tianshan No. 1	Region II	43.12	86.82	Tien Shan	Snow, dust	4063	0.719404–0.721728	-10.9–-6.9	Nagatsuka et al., 2010; Xu et al., 2012
4	Miaoergou		43.06	94.32	Tiean Shan	Snow, Ice, Cryoconite	3100–4512	0.710284–0.720825	-11.6–-7.3	Du et al., 2015; Wei et al., 2019
5	Yuzhufeng Glacier		35.66	94.24	Kulun	Snow	4300–4720	0.714821–0.716757	-16.6–-11.8	Wei et al., 2019
6	Zangsegangri		34.27	85.85	Qiangtang	Snow	6226	0.717352–0.718328	-12.9–-9.2	Xu et al., 2012
7	Guoqu	Region III	33.58	91.20	Tanggula	Snow	5765	0.717546–0.721786	-10.2–-9.5	Xu et al., 2012
8	Dongkemadi		33.10	92.10	Tanggula	Snow	5700	0.713192	-10.5	Xu et al., 2012
9	Zadang		30.47	90.65	Nyainqentanglha	Snow	5758	0.718285–0.721305	-12.9–-11.1	Xu et al., 2012
10	Jiemyangzong		30.22	82.17	Himalaya	Snow	5558	0.72671–0.740694	-14.3–-10.5	Xu et al., 2012
11	Yala	Region IV	28.23	85.62	Himalaya	Snow	5190	0.740112	-15.68	Xu et al., 2012
12	East Rongbuk		28.10	86.97	Himalaya	Snow	6525	0.728057–0.757407	-28.1–-14.7	Xu et al., 2012
13	Laohugou Glacier No.12		39.43	96.53	Qilian	Snow	4288–5026	0.720448–0.723303	-15.7–-9.5	Xu et al., 2012; Wei et al., 2019
14	Dunde ice cap		38.10	96.40	Qilian	Ice	5325	0.715220–0.721874	-11.1–-9.9	Wu et al., 2010
15	Qiyi Glacier 1	Region V	39.24	97.76	Qilian	Snow	4500–4750	0.712349–0.722751	-13.7–-8.6	Dong et al., 2018
16	Shiyi Glacier		38.21	99.88	Qilian	Snow	3928–4152	0.721032–0.721711	-14.0–-13.8	Wei et al., 2019
17	Dabanshan		37.36	101.40	Qilian	Snow	3593–3625	0.723105–0.725015	-12.1–-12.0	Wei et al., 2019
18	Lenglongling Glacier		37.52	101.90	Qilian	Snow	3558–3992	0.719084–0.728414	-10.9–-7.0	Dong et al., 2018
19	Dagu Glacier		32.12	102.43	Hengduan	snow	3520–3701	0.719216–0.721102	-16.9–-12.3	Dong et al., 2018
20	Hailuogou Glacier	Region VI	29.33	101.57	Hengduan	snow	3010–3850	0.722805–0.728326	-17.1–-12.0	Dong et al., 2018
21	Demula Glacier		29.37	97.00	Hengduan	Snow	5404	0.729095–0.735863	-17.1–-14.2	Xu et al., 2012
22	Baishui Glacier No.1		27.10	100.20	Hengduan	Snow	4338–4747	0.717145–0.719881	-13.8–-11.4	Xu et al., 2012; Dong et al., 2018

807

808

809

810

811

812

813

814

815

816 Table 3. Snow, cryoconite, sand, soil and sediment samples located in the Arctic. Headers from left to
 817 right: Label; Subregions; name of the sampling site where the samples were taken; Sample type: Snow,
 818 Cryoconite, sand and soil; Ref.: reference publications.

Label	Subregion	Location	Sample type	Time interval	Size fraction	Ref
1	GrISS	East GrIS; North GrIS	snowpit	2017/2018; early-1995	>0.2 μm ; <45 or 38 μm	This study; Bory et al., 2002
2	GrIS-S	East GrIS; West GrIS	Cryoconite, Moraine, Englacial dust, Sand, Rock, Sediment	NO	Bulk	This study; Nagatsuka et al., 2016; Simonsen et al., 2019
3	SV	Ny-Ålesund	Snow, Sand, Soil; Sediment	NO	Bulk; <100 μm	Tütken et al., 2002; Maccali et al., 2018; Du et al., 2019b
4	AO	Arctic Ocean	Snow	2016	Bulk	This study; Du et al., 2019b
5	AOSI	Arctic Ocean	Sea ice sediment	NO	<100 μm	Eisenhauer et al., 1999; Tütken et al., 2002
6	AOSed	Arctic Ocean	Sediment	NO	Bulk; <100 μm	Eisenhauer et al., 1999; Tütken et al., 2002; Maccali et al., 2018
7	BS	Arctic Ocean	Sediment	NO	<100 μm	Tütken et al., 2002; Maccali et al., 2018
8	KS	Arctic Ocean	Sediment	NO	<100 μm	Tütken et al., 2002; Maccali et al., 2018
9	LS	Arctic Ocean	Sediment	NO	<100 μm ; Bulk	Eisenhauer et al., 1999; Maccali et al., 2018
10	ESS	Arctic Ocean	Sediment	NO	<100 μm	Bazhenova et al., 2017; Maccali et al., 2018
11	BCS	Arctic Ocean	Sediment	NO	<100 μm ; Detrital	Asahara et al., 2012; Bazhenova et al., 2017; Maccali et al., 2018; Du et al., 2019b
12	CAA	Arctic Ocean	Sediment	NO	<100 μm	Asahara et al., 2012; Bazhenova et al., 2017; Maccali et al., 2018

819